Performance of columns packed with the new shell particles, Kinetex-C$_{18}$

Fabrice Gritti [a], Irene Leonardis [a], David Shock [b], Paul Stevenson [b], Andrew Shalliker [b], Georges Guiochon [a,*]

[a] Department of Chemistry, University of Tennessee, Knoxville, TN 37996-1600, USA
[b] Australian Centre for Research on Separation Science, University of Western Sydney, NSW, Australia

ARTICLE INFO

ABSTRACT

The performance of the new Kinetex-C$_{18}$ column was investigated. Packed with a new brand of porous shell particles, this column has an outstanding efficiency. Once corrected for the contribution of the instrument extra column volume, the minimum values of the reduced plate heights for a number of low molecular weight compounds (e.g., anthracene and naphtho[2,3-a]pyrene) were between 1.0 and 1.3, breaking the legendary record set 3 years ago by Halo-C$_{18}$ packed columns. The liquid-solid mass transfer of proteins (e.g., insulin and lyzozyme) is exceptionally fast on Kinetex-C$_{18}$ much faster than on the Halo-C$_{18}$ column. The different contributions of dispersion and mass transfer resistances to the column efficiency were determined and discussed. The possible reasons for this extremely high column efficiency are discussed.

© 2010 Elsevier B.V. All rights reserved.

1. Introduction

After more than 20 years of near stagnation, packed column technology has begun rapidly to evolve in the last 10 years. The first, monolithic columns appeared at the turning of the last century, threatening the monopoly of columns packed with particles but slowly losing momentum. Then, the average particle size routinely used in commercial columns began progressively to decrease, first from 5 to 3 μm and lately to sub-2 μm particles [1]. Columns packed with the latter particles allowed to reach high resolution power with reduced plate heights as low as 3.2 μm (i.e., ca. 300,000 plates per meter) for small molecules [2] and to reduce analysis times by ca. one order of magnitude. The main disadvantage of such columns is the need for suitable instruments that are capable of operating at pressure as high as 15,000 psi (1000 bar) and to record without significant distortion the very narrow peaks eluted from the columns

[3]. In about the same time when sub-2 μm particles were commercialized, other scientists search to prepare particles that are large enough to be used at velocities somewhat larger than their optimum velocity for maximum efficiency and exhibit low mass transfer resistance. This combination can provide columns that can be operated with conventional pumps but have efficiency comparable to that of columns packed with sub-2 μm particles. Three years ago, Kirkland obtained the superficially porous or shell Halo-C$_{18}$ particles [4–8]. This exceptionally performing material was made of 1.7 μm solid silica core covered by a 0.5 μm porous silica shell. It provided minimum reduced HETPs of ca. 1.5 for small molecular weight compounds [9], a significant improvement in packed column technology since the minimum reduced HETP of totally porous particle is usually of the order of 2.0.

The mass transfer mechanism in Halo-C$_{18}$ packed columns was investigated from a theoretical [10,11] and an experimental point of view [9,12]. Inverse size exclusion chromatography (ISEC) data show that the external porosity of these columns is slightly larger than that of totally porous particles (0.42 vs. 0.37) [9]. It was suggested that this high porosity is due to the external roughness of the surface of the shell and a high friction forces between the particles, hence to the formation of a chromatographic bed with a relatively low density but a high degree of radial homogeneity. The

* Corresponding author at: Department of Chemistry, University of Tennessee, 413 Buehler Hall, Knoxville, TN 37996-1600, USA. Tel.: +1 865 974 0733; fax: +1 865 974 2667.
E-mail addresses: guiochon@utk.edu, guiochon@ion.chem.utk.edu (G. Guiochon).

reduced B term in the van Deemter equation of Halo columns is smaller than that of conventional porous particles ($\simeq -25\%$) and is easily explained by the smaller internal porosity of the particles, which provides a smaller volume accessible for sample diffusion [9]. Finally, the reduced C term measured for Halo-C_{18} particles for small molecular weight compounds was not significantly different from that of the totally porous particles, probably because the C term depends mostly on the external film mass transfer resistance and the eddy dispersion term [13]. The effective intraparticle sample diffusivity of small molecules is so fast that the mass transfer resistance through either conventional or superficially porous particles is negligible [14]. Finally, the low reduced A term measured on the Halo columns is in part due to the very narrow particle size distribution, with a relative standard deviation around 5% *vs.* 20% for most totally porous particles, and probably in part by the high friction coefficient between particles caused to their surface roughness, which decreases the amount of strain taking place during consolidation of the packed bed. It does not seem to be related to unusually small transcolumn mobile phase velocity gradients. The measurement of the local flow velocity across the column diameter by electrochemical detection [12] demonstrated that the amplitude of the flow velocity gradient across the column diameter of columns packed with either totally or superficially porous particles was comparable. Overall, the commercially available Halo columns packed with 2.7 μm superficially porous particles has provided under the best conditions minimum reduced HETPs as small as 1.4, a level of separation power never approached earlier by any conventional packing material.

A first goal of this work was to assess the performance of columns packed with particles of a new brand of shell particles, Kinetex-C_{18} by Phenomenex, in which a solid core is wrapped in a porous layer or shell of a silica adsorbent. Nearly 3 years ago, a first generation of shell particles established a landmark record for the minimum reduced HETP. Columns packed with Halo-C_{18} particles that have characteristics similar to those of the Kinetex-C_{18} particles were the most suitable term of comparison in the present study. In a first part, we report on measurements of the height equivalent to a theoretical plate (HETP) of conventional chemicals, a peptide and two proteins in a wide range of mobile phase velocity and discuss the different contributions to mass transfer resistance.

For the last 40 years, HPLC has been a vast battlefield on which column producers faced instrument manufacturers. The specifications of the first group were often met late, rarely completely, and often grudgingly by the latter. Analysts want faster separations and better resolutions. Physical chemists explain that this can be achieved only with shorter columns, packed with finer particles, and fed by more powerful pumps. Instrument designers struggle to meet the new specifications. Then, column producers develop a new generation of particles, finer, more performing, and a new set of instrument specifications is written and the fights resume. The most difficult source of problems was always the recurrent difficulty at reducing the extra column contributions to band broadening, the most important of which are the dispersion caused by the extra column volumes and the deformation of the band profiles due to the response time of detectors and by the limited frequency of acquisition of digital data. Other major battles in this war were fought around issues of accuracy, precision, reliability. They were less sharp and progress there came more often through incremental but steady improvements rather than through major changes in instrument design.

The advent of the first generation of fine shell particles exemplified by the Halo column gave a warning that a new battle was shaping up. The advent of the second generation of shell particles opens the new war and sends a new generation of engineers to the drawing-board or rather the computer assisted design programs. The second goal of this paper is to attempt first to assess the impact of the currently available instruments on the overall, practical performance of the new generation of columns and finally to sketch what could be the specifications for a new generation of instruments for HPLC.

2. Theory

2.1. Reduced linear velocity

In all this work, we report on measurements of efficiency data of a Kinetex-C_{18} column. We express these data as the reduced plate height $h = H/d_p$ of the column (with H column HETP and d_p average particle size) and we discuss the variations of h as a function of the reduced interstitial velocity ν. By definition,

$$\nu = \frac{u d_p}{D_m} \tag{1}$$

where D_m is the bulk molecular diffusivity, and u is the interstitial linear velocity, which is given by:

$$u = \frac{F_\nu}{\epsilon_e \pi R_c^2} \tag{2}$$

where F_ν is the volume flow rate of the mobile phase, ϵ_e is the interstitial porosity, and R_c is the inner radius of the column tube.

The molecular diffusivities of the low-molecular-weight compounds used here (anthracene and naphtho[2,3-a]pyrene) were estimated using the classical Wilke and Chang equation [15]:

$$D_m = 7.4 \times 10^{-8} \frac{(\Psi M_S)^{0.5} T}{\eta V_A^{0.6}} \tag{3}$$

where Ψ is the solvent association factor ($\Psi = 1$ for pure acetonitrile [16]), M_S the molecular weight of the mobile phase (g/mol), η its viscosity ($\eta = 0.37$ cP for pure acetonitrile at 295 K), T is the temperature, and V_A is the molar volume of the solute at its boiling point (cm^3/mol). V_A was estimated according to the group method of Schroder and Lebas [16].

The molecular diffusivity of the peptide (bradykinin) was estimated using the correlation of Young et al. [17]:

$$D_m = 8.34 \times 10^{-8} \frac{T}{\eta M^{(1/3)}} \tag{4}$$

The two correlations in Eqs. (3) and (4) give reasonable values of D_m for the compounds used in this work. The diffusion coefficients of anthracene, naphtho[2,3-a]pyrene, and bradykinin were estimated at 1.6×10^{-5}, 1.2×10^{-5}, and 2.32×10^{-6} cm^2/s, respectively. The molecular diffusivities of the proteins insulin (1.63×10^{-6} cm^2/s) and lyzozyme (1.20×10^{-6} cm^2/s) were directly taken from experimental data available in the literature [18,19].

2.2. The Mass transfer resistances

The overall reduced HETP of a chromatographic column is the sum of three main contributions due to longitudinal diffusion (the B term), eddy dispersion (the A term), and overall solid-liquid mass transfer resistance (the C term), as described in the general empirical van Deemter plate height equation [20].

$$h = \frac{B}{\nu} + A + C\nu \tag{5}$$

More elaborate kinetic models account for the actual structure of the packed chromatographic bed, including the moving eluent in the interparticle space, the stagnant eluent in the mesopore network inside the porous particles, and the solid stationary phase. First Giddings [21], later Horvath and Lin [22,23], and finally Guiochon et al. [24] elaborated different sophisticated plate height equations. These equations have been reviewed and compared

elsewhere [25,26]. They are written as the sum of four different contributions:

$$h = h_{Long.} + h_{Eddy} + h_{Film} + h_{Particle} \tag{6}$$

2.2.1. First, the reduced longitudinal diffusion term

In the term ($h_{Long.}$), the role actually played by the stationary phase is not negligible, due to the important role of surface diffusion in the adsorbed state [27]. The contribution $h_{Long.}$ is written:

$$h_{Long.} = 2\frac{\gamma_e + ((1-\epsilon_e)(1-\rho^3)/\epsilon_e)\Omega}{\nu} \tag{7}$$

where γ_e is the obstruction factor for diffusion in the interparticle volume (γ_e is of the order of 0.60 [28]), Ω is the ratio of the intra-particle diffusivity of the sample through the porous silica-C_{18} shell (D_{shell}) to the bulk diffusion coefficient (Ω is of the order of unity for small molecules [29]), and $\rho = R_i/R_e$ is the ratio of the diameter of the solid core to that of the particle, with $\rho = 0.73$ and 0.63 for the Kinetex-C_{18} and Halo-C_{18} particles, respectively.

2.2.2. Second, the eddy dispersion term

This term, h_{Eddy}, results from the combination of various sources of flow heterogeneity inside the packed column. This includes sources of four different origins, differing in the length scale considered, e.g., the transchannel ($i = 1$), the short-range interchannel ($i = 2$), the long-range interchannel ($i = 3$), and the transcolumn flow heterogeneities ($i = 4$). At high reduced interstitial velocity, eddy dispersion is essentially controlled by a flow mechanism and a general expression is given by [21,30]:

$$h_{Eddy} = \sum_{i=1}^{i=4} \frac{1}{(1/2\lambda_i) + (1/\omega_i\nu)} \simeq 2\sum_{i=1}^{i=4}\lambda_i \tag{8}$$

The values of λ_1, λ_2, and λ_3 in Eq. (8) were estimated by Giddings more than 50 years ago. These estimates are still valid today for columns packed with modern very fine particles [21]. Their values are based on quantitative estimates made for the different velocity inequalities $\omega_{\beta,i}$ and for the axial convection lengths $\omega_{\lambda,i}$:

$$\lambda_i = \frac{\omega_{\beta,i}^2 \omega_{\lambda,i}}{2} \tag{9}$$

For the transchannel mechanism, $\omega_{\beta,1} = 1$ and $\omega_{\lambda,1} = 1$. For the short-range interchannel mechanism, $\omega_{\beta,2} = 0.8$ and $\omega_{\lambda,2} = 1.5$. For the long-range interchannel mechanism, $\omega_{\beta,3} = 0.2$ and $\omega_{\lambda,3} = 5$. So, as a first guess, $\lambda_1 = 0.5$, $\lambda_2 = 0.5$, and $\lambda_3 = 0.1$. The value of λ_4 is derived from the flow distribution across the column diameter. Quartic flow profile distributions have been observed [50] and the following expression of the parameter λ_4 was recently derived [30]:

$$\lambda_4 = \frac{2}{45}\frac{L}{d_p}\omega_{\beta,c}^2 \tag{10}$$

where $\omega_{\beta,c}$ is the relative flow velocity difference between the center and the wall of the column and L is the column length. Assuming $\omega_{\beta,c} = 1\%$, $L = 15$ cm, and $d_p = 3$ μm then $\lambda_4 = 0.22$.

2.2.3. Third, the external film mass transfer term

This term, h_{Film}, was derived from the Laplace transform of the general rate model equations [24]. It is written:

$$h_{Film} = \frac{\epsilon_e}{1-\epsilon_e}\frac{k_1^2}{(1+k_1)^2}\frac{1}{3Sh}\nu \tag{11}$$

where $Sh = (k_f d_p/D_m)$ is the Sherwood number, k_f is the film mass transfer coefficient, and k_1 is given for superficially porous particles by [10]:

$$k_1 = \frac{1-\epsilon_e}{\epsilon_e}\left(\epsilon_p + \frac{1-\epsilon_p(1-\rho^3)}{1-\rho^3}K_a\right)(1-\rho^3) \tag{12}$$

where ϵ_p is the porosity of the porous shell of the particle and K_a is the Henry's constant of adsorption on the walls of the porous shells. The relationship between the measurable retention factor k' and the Henry's constant K_a is:

$$k' = \frac{1-\epsilon_t}{\epsilon_t}K_a \tag{13}$$

where ϵ_t is the total porosity of the column. The Sherwood number can be estimated from the Wilson and Geankoplis correlation [31]:

$$Sh = \frac{1.09}{\epsilon_e^{(2/3)}}\nu^{(1/3)} \tag{14}$$

2.2.4. Fourth, the contribution of the transparticle mass transfer resistance

Finally, in Eq. (6), the term $h_{Particle}$ is given by the following equation, previously derived for shell particles [10]:

$$h_{Particle} = \frac{\epsilon_e}{1-\epsilon_e}\frac{k_1^2}{(1+k_1)^2}\frac{1}{30\Omega}\frac{1+2\rho+3\rho^2-\rho^3-5\rho^4}{(1+\rho+\rho^2)^2}\nu \tag{15}$$

This equation is consistent with the one derived previously for totally porous particles when $\rho = 0$. As ρ increases (e.g., as the diameter of the solid core increases), the apparent intraparticle diffusivity of the probe studied increases and the mass transfer kinetics becomes faster through the shell particles than it is through totally porous particles. In theory, for large Henry's constant K_a, the intraparticle diffusivity of the Kinetex-C_{18} ($\rho = 0.73$) and the Halo-C_{18} particles ($\rho = 0.63$) should be 2.3 and 1.7 times larger, respectively, than the apparent diffusivity in fully porous particles of the same size.

3. Experimental

3.1. Chemicals

The mobile phase used in this work was made of either pure acetonitrile or a mixture of water and acetonitrile. Dichloromethane ($\rho_{CH_2Cl_2} = 1.306$ g/cm^3) and isopropanol ($\rho_{iPrOH} = 0.782$ g/cm^3) were used in markedly smaller amounts, to measure the column hold-up volumes by pycnometry. These four solvents were HPLC grade from Fisher Scientific (Fair Lawn, NJ, USA). The mobile phase was filtered before use on a surfactant-free cellulose acetate filter membrane, 0.2 μm pore size (Suwannee, GA, USA). Trifluoro acetic acid, anthracene, naphtho[2,3-a]pyrene, and lyzozyme were purchased from Aldrich (Milwaukee, WI, USA). Bradykinin was ordered from American Peptides Company Inc. (Sunnyvale, CA). Insulin was a generous gift from Ely Lilly (Indianapolis, IN, USA). Eleven polystyrene standards (MW = 590, 1100, 3680, 6400, 13,200, 31,600, 90,000, 171,000, 560,900, 900,000, and 1,877,000) were used to acquire inverse size exclusion chromatography data (ISEC). They were purchased from Phenomenex (Torrance, CA, USA).

3.2. Columns

The new Kinetex-C_{18} column (100 mm × 4.6 mm) was a generous gift from the column manufacturer (Phenomenex, Torrance, CA, USA). The Halo-C_{18} column (150 mm × 4.6 mm) was purchased from Advanced Material Technology (Wilmington, DE, USA). The main characteristics of the bare porous silica and those of the final derivatized packing material are summarized in Table 1.

Table 1
Physico-chemical properties of the Kinetex and Halo columns given by the manufacturer and measured in our lab. [a,b,c]

Neat silica	Halo	Kinetex
Particle size (μm)	2.7	2.5
$\rho = R_i/R_e$	0.63	0.73
Pore diameter (Å)	90	96
Surface area (m^2/g)	127	200
Particle size distribution ($d_{90-10\%}$)	1.14	1.12
Bonded phase analysis	Halo-C$_{18}$	Kinetex-C$_{18}$
Total carbon (%)	7.5	12
Surface coverage (μmol/m^2)	4.0 (C$_{18}$ + endcapping agent)	2.7 (C$_{18}$ only)
Endcapping	Yes	Yes
Packed columns analysis	Lot number/serial number	
	AH092221/USFH002149	5569-76/496449
Dimension (mm × mm)	4.6×150	4.6×100
External porosity [a]	0.391	0.372
Total porosity [b]	0.532	0.542
Particle porosity [d]	0.232	0.271
Shell porosity	0.309	0.444
Average particle size [c] ($K_c = 180$)	2.70	2.48
Specific permeability k_0 (cm^2)	6.53×10^{-11}	4.46×10^{-11}

[a] Measured by inverse size exclusion chromatography (polystyrene standards).
[b] Measured by pycnometry (IPrOH–CH$_2$Cl$_2$).
[c] Measured from the column back pressure data corrected for extra-column contributions and the Kozeny–Carman Eq. 18 ($K_c = 180$).
[d] The particle porosity includes the volume of the solid silica core.

3.3. Apparatus

The data were acquired with a HP1090 (Agilent Technology, Wilmington, DE, USA) and an Acquity UPLC (Waters, Milford, MA, USA) liquid chromatographs.

The HP1090 instrument includes a multi-solvent delivery system (with three 1-L tanks), an auto-sampler with a 250 μL sample loop (injection of 5 μL), a column thermostat, a diode-array UV-detector (1.7 μL, sampling rate set at 25 Hz), and a data station. Compressed nitrogen and helium bottles (National Welders, Charlotte, NC, USA) were connected to the instrument to allow continuous operations of the pump, the auto-sampler, and the solvent sparging. The overall extra-column volume was 39.6 μL from the injection seat of the auto-sampler to the detector cell, measured as the apparent hold-up volume of a zero-volume union connector in place of the column. The maximum flow rate and inlet pressure that can be applied are 5.0 mL/min and 400 bar, respectively.

The Acquity UPLC instrument includes a quaternary solvent delivery system, an auto-sampler with a 5 μL sample loop (injection of 1 μL, sample loop option : partial loop with needle overfill), a monochromatic UV detector (0.5 μL, sampling rate set at 40 Hz), a column oven, and a data station running the Empower data software from Waters. From the exit of the Rheodyne injection valve to the column inlet and from the column outlet to the detector cell, the total extra-column volume of the instrument is 15.6 μL, measured as indicated above. A time offset of 0.71 s was measured after the zero injection time was recorded. The maximum flow rate and pressure that can be applied during an acquisition run are 2.0 mL/min and 732 bar, respectively.

The HETP vs. mobile phase flow velocity curves were determined by running the following sequence of mobile phase velocities: 0.1, 0.2, 0.3, 0.4, 0.5, 0.6, 0.7, 0.8, 0.9, 1.0, 1.2, 1.4, 1.6, 1.8, 2.0 (UPLC instrument limit), 2.2, 2.4, 2.6, 2.8, and 3.0 mL/min (20 data points maximum). The flow rates of 2.2, 2.4, 2.6, 2.8, and 3.0 mL/min were only applied on the HP1090 chromatograph. The HETP measurements were made at each flow rate in triplicate; the average of the three data points is reported in the following figures at each veloc-

ity corresponding to these flow rates. The column inlet pressures measured at a flow rate of 3 mL/min were 262 and 300 bar with the 10 cm long Kinetex and the 15 cm long Halo columns, respectively.

The flow rate accuracy was determined by directly pumping the pure mobile phase at 295 K and 0.1, 1, and 2.5 mL/min during 50, 50, and 20 min, respectively. The relative error was always less than 0.5% (HP1090) and 0.2% (Acquity UPLC), so we estimate the long-term accuracy of the flow-rate at 4 μL/min or better at flow rates around 1 mL/min. The laboratory temperature was controlled by an air conditioning system set at 295 K. The daily variation of the ambient temperature never exceeded $\pm 1°$C.

All chromatographic separations were performed on a Shimadzu LC system, incorporating a LC-10ATvp pumping system, a SIL-10ADvp auto injector, a SPD-10Avp UV detector (set at 254 nm; co-eluting peaks were distinguished by choosing another appropriate wavelengths), and Shimadzu Class-VP software on a Pentium II 266 MHz processor.

3.4. Measurement of the HETP data

The injected sample volume were 5 and 1 μL on the HP1090 and the Acquity UPLC instruments, respectively. The samples were acetonitrile solutions, highly dilute in order to maintain linear the adsorption isotherms of these probes. The concentrations of anthracene, naphtho[2,3-a]pyrene, bradykinin, insulin, and lyzozyme were 0.045, 0.037, 0.2, 0.2, and 0.2 g/L, respectively. The detection wavelengths were set to 358, 294, 205, 205, and 205 nm, respectively. The mobile phases were pure acetonitrile for both anthracene and naphtho[2,3-a]pyrene. Mixtures of water, acetonitrile, and trifluoro-acetic acid were used for the elution of lyzozyme (35/65/0.1, v/v/v), insulin (31/69/0.1, v/v/v), and bradykinin (23/77/0.1, v/v/v).

The peak profile data were acquired at frequencies of 25 Hz with the HP1090 and 40 Hz with the Acquity. The extra-column contributions to the retention volume and to the band broadening of probes were measured by replacing the chromatographic column with a zero-volume capillary restrictor, the contribution of which to the column back pressure was of the same order of magnitude as that of the column.

The experimental HETP data were corrected for the contributions of the extra-column volumes. For that purpose they were calculated with the following equation:

$$H = L \frac{\left(t_{1/2}^r - t_{1/2}^f\right)^2 - \left(t_{1/2,e}^r - t_{1/2,e}^f\right)^2}{5.545(t_R - t_e)^2} \quad (16)$$

where t_R and t_e are the retention times recorded for the peak apices of the probe compound with and without a column fitted on the instrument, $t_{1/2}^r$ and $t_{1/2,e}^r$, and $t_{1/2}^f$ and $t_{1/2,e}^f$ are the rear and the front widths of the peak measured at half-height of the peak. The precision of the measurement of the HETPs remains within 12%.

For both instruments the extra-column volume peak variance, $\mu_{2,ex}'$, expressed in μL^2 was calculated as follows:

$$\mu_{2,ex}' = F_v^2 \frac{\left(t_{1/2,e}^r - t_{1/2,e}^f\right)^2}{5.545} \quad (17)$$

where the flow rate F_v is expressed in μL/min and the elution times $t_{1/2,e}$ in minutes.

The extra-column contributions were measured with the same mobile phases and the same compounds as those that were used when the chromatographic column was fitted to the instrument. The column was merely replaced by a zero-volume connector.

4. Results and discussion

We first discuss some important characteristics (external, inter-particle porosity and permeability) of the two columns studied. Then, we report on the HETP plots of a series of samples measured on these columns under the very same conditions and we compare their performance.

4.1. External porosity and permeability of the Kinetex-C_{18} and Halo-C_{18} columns

The external porosity ϵ_e of each column was derived from ISEC measurements. As previously explained, ϵ_e is directly derived from the extrapolation of the exclusion branch of the ISEC plot [9], or plot of the column volume accessible to a polystyrene standard vs. the cubic root of its molecular weight. Fig. 1A and B show these plots for the Kinetex-C_{18} and the Halo-C_{18} columns, respectively. First, we observe that the total porosities of both columns are close to 0.54, a porosity value that is relatively low for conventional packed columns. The smaller than usual volume of eluent in these columns is the direct consequence of the solid core in these particles, which
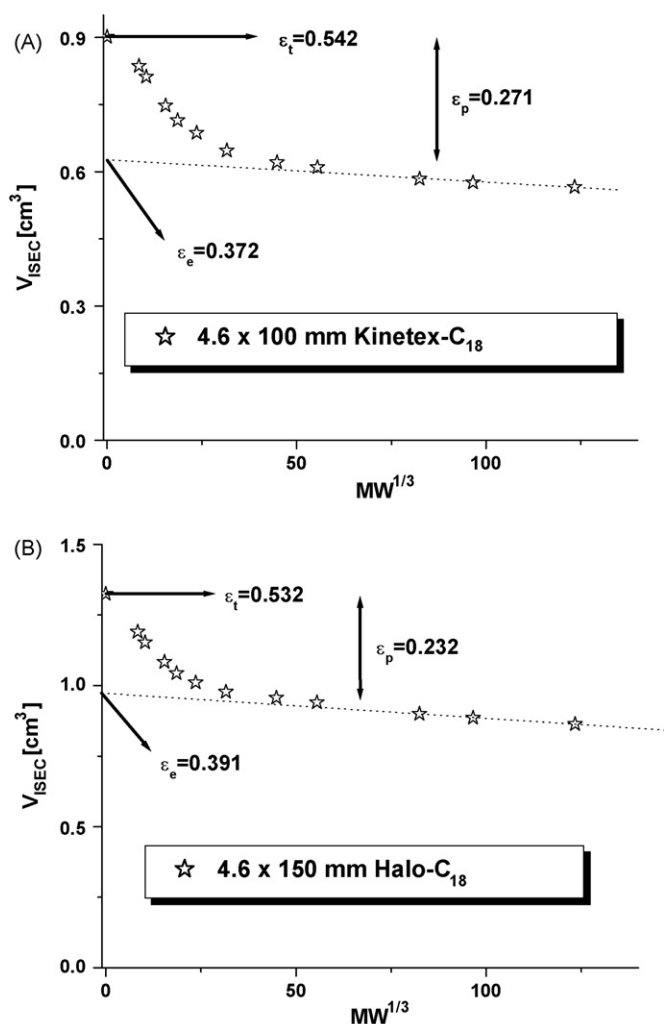

Fig. 2. Permeability data of Kinetex-C_{18} and Halo-C_{18} columns. Plots of column pressure drop, ΔP (corrected for the contribution of the extra-column volumes) vs. the superficial flow velocity, u_S, with pure acetonitrile, viscosity taken at $T = 295$ K and $P = P^0$: 0.37 cP. Flow rate range: 0.1 to 3.0 mL/min. The average particle diameters are derived from the Kozeny–Carman relationship (see equation for the permeability k_0 given in the graph).

causes the internal porosity of the particles to be smaller than 0.30 (in contrast, fully porous particles have an internal porosity of 0.40 or more). Second, the external porosities of both columns are very similar to those of columns packed with totally porous particles (ϵ_e is almost always within the range 0.35–0.40). We found values of $\epsilon_e = 0.372$ and 0.391 for the Kinetex and the Halo columns, respectively. Thus, the Kinetex-C_{18} particles seem to be slightly more densely packed than the Halo-C_{18} particles, possibly because the former column is shorter than the latter. However, the precision of ISEC experiments does not exceed a few percent, so the difference observed are not significant. Finally, the SEM photographs show that the external surface of these shell particles is rougher than that of the classical totally porous particles [32].

From the values of the external porosity, we can estimate the average particle size by measuring the permeability constant of these two columns. Fig. 2 shows the variation of the column pressure drop ΔP (the inlet pressures were corrected for the extra-column back pressures) when increasing the superficial linear velocity u_S. The Kozeny–Carman relationship provides a theoretical framework between these two variables, which is written [21]:

$$\frac{\Delta P}{L} = \eta \frac{K_c(1-\epsilon_e)^2}{\epsilon_e^3 d_p^2} u_S \tag{18}$$

where K_c is the Kozeny–Carman constant. Its numerical value is usually close to 180 for packed beds of spherical particles [21]. From the slope of the plots shown in Fig. 2, we can estimate the average particle size, d_p, assuming that $K_c = 180$ in Eq. (18). The viscosity η of pure acetonitrile at 295 K is taken as 0.37 cP. The external porosities ϵ_e are those measured by ISEC. The values obtained for d_p are 2.48 and 2.70 μm for the Kinetex-C_{18} and the Halo-C_{18} columns, respectively, in excellent agreement with the average particle sizes measured by the Coulter method and provided by the manufacturers (see Table 1). This agreement is not surprising since we already knew the spherical shape of these shell particles and their very narrow particle size distribution (PSD). For instance, the 90/10% ratio of the PSD of Kinetex-C_{18} and Halo-C_{18} particles are 1.12 and 1.14, respectively, according to the manufacturer data (Table 1).

4.2. Performances of the Kinetex and Halo columns

The efficiencies of the two columns were measured for five different probe compounds with molecular masses of 178 g/mol

Fig. 1. ISEC measurements. Eluent: pure tetrahydrofuran. Flow rate: 0.25 mL/min. $T = 295$ K. Plots of the elution volumes of 11 polystyrene standards vs. the cubic root of their known average molecular weights ($MW^{1/3}$). Two columns packed with two brands of shell particles were studied. (A) Kinetex-C_{18} column. (B) Halo-C_{18} column. The external porosities, ϵ_e, were extrapolated at $MW = 0$ from the excluded ISEC branch of each plot (dotted lines). The single data point for $MW = 0$ was measured by pycnometry.
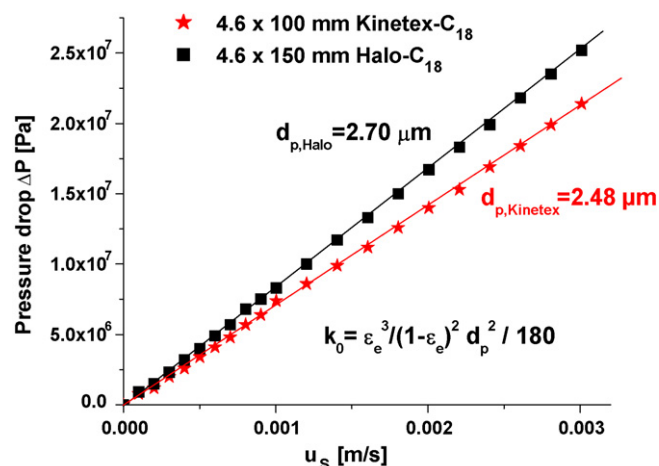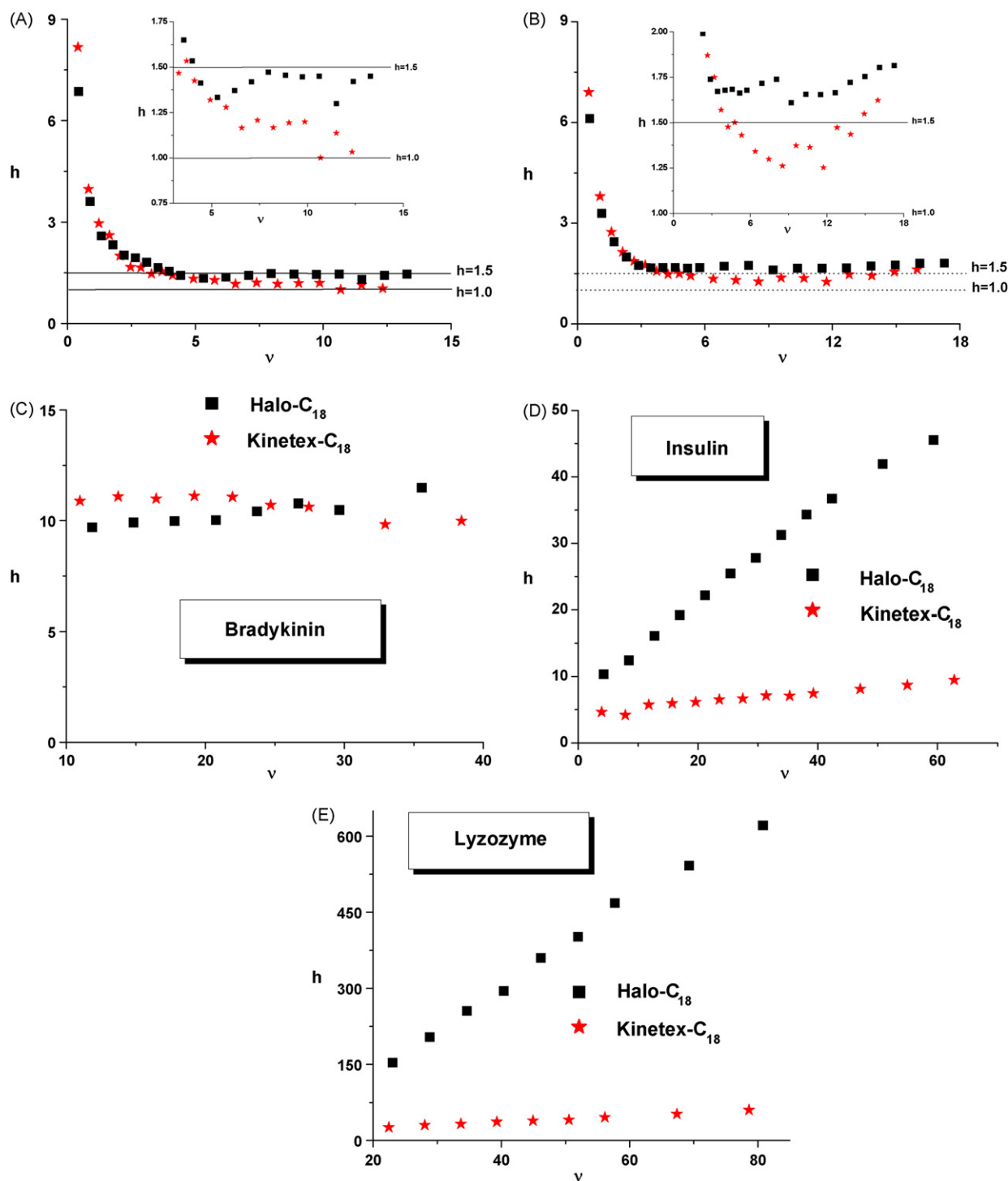
Fig. 3. Reduced HETPs of a series of five samples measured on the Kinetex (full stars) and on the Halo (full squares) columns. $T = 295$ K. (A) Anthracene. Eluent: pure acetonitrile. The insert graph zooms in the high reduced linear velocity region in order to appreciate better the difference between the HETP data of each column. (B) Same as in (A), except the sample is naphtho[2,3-a]pyrene. (C) Same as in (A) except the sample is bradykinin and the eluent is a mixture of water, acetonitrile, and TFA (23/77/0.1, v/v/v). (D) Same as in (A), except the sample is Insulin and the eluent is a mixture of water, acetonitrile, and TFA (31/69/0.1, v/v/v). (E) Same as in (A), except the sample is lyzozyme and the eluent a mixture of water, acetonitrile, and TFA (37/63/0.1, v/v/v).

(anthracene), 302 g/mol (naphtho[2,3-a]pyrene), 1059 g/mol (bradykinin), 5800 g/mol (monomeric insulin), and 14,300 g/mol (lysozyme). The bulk diffusion coefficients of these compounds are 1.56×10^{-5}, 1.20×10^{-5}, 2.32×10^{-6}, 1.63×10^{-6}, and 1.20×10^{-6} cm²/s, respectively, at 295 K and in their respective eluents. The rational behind the commercialization of the shell particles is that the mass transfer resistances should be

less through shell particles than through fully porous particles because the probe molecules have a shorter migration distance in the former case (see Eq. (15)). The advantage of shell particles should become important when very large analytes, such as biopolymers, are analyzed because the latter compounds diffuse slowly through the porous structure of the particles.

Fig. 3A–E show plots of the reduced efficiency of the Kinetex-C_{18} and the Halo-C_{18} columns *vs.* the mobile phase reduced velocity for anthracene, naphtho[2,3-a]pyrene, bradykinin, insulin, and lysozyme, respectively in the corresponding mobile phases (see Section 3.4).

4.2.1. Efficiency for small molecules

Fig. 3A shows plots of the reduced HETP of anthracene on the Halo-C_{18} (full black squares) and on the Kinetex-C_{18} (full red stars) columns. Pure acetonitrile was used because its viscosity is very low, which permits the achievement of the highest possible eluent flow rates with any given instrument. Since diffusion processes are scaled to the bulk diffusion coefficients, mass transfers are the fastest, so the lowest HETP are measured at any given high flow rate. This eluent was also used in previous reports to study the performance of columns packed with sub-2 μm totally porous particles [2]. For the sake of consistency and fair comparison between the different particle technologies, we conserved pure acetonitrile as our main mobile phase. The reduced HETP data given in Fig. 3A were corrected from the extra-column volume contributions of the HP1090 chromatograph (these contributions are 40 μL and 39 μL^2 for the first and second central moments, respectively, at a flow rate of 0.5 mL/min). First, it is noteworthy that the two columns have close *B* term values (slightly larger on the Kinetex column, by about + 16%). This result is not surprising given the similarity between the structure (poroshell) of the two columns and the closeness of the retention factors of anthracene ($k' \simeq 0.4$ and 0.5 on Kinetex and Halo columns, respectively). Second, as expected, the values of the *C* term on either column is barely significantly different from 0 and the HETP barely increases in the range of reduced velocity investigated (5–13). This is in part due to the large diffusion coefficient of anthracene. Most interestingly, at high reduced linear velocities, the HETP depends essentially on the contribution of eddy diffusion, i.e., on the value of the *A* term of the columns. Reduced HETP values as small as 1.4 and 1.1 were observed for the Halo and the Kinetex column, respectively. Experimental minimum reduced HETPs of 1.4 for the Halo column have already been reported in both the RPLC [9] and the HILIC [33] modes. Our result confirms the values of these earlier measurements, made on different columns, hence, the reproducibility of the Halo column. It also proves that our measurements are accurate. So far, a minimum HETP of 1.4 represented the best performance of practical interest ever achieved in column manufacturing technology (i.e., the best combination of excellent particle preparation and outstanding column packing technologies). Smaller plate heights have been reported in GC for 1 mm i.d. columns packed with 0.2 mm glass beads by Knox and Parcher as early as 1969 [34]. Similar results were occasionally reported under exceptional conditions, e.g., with narrow bore tubes packed with particles having a diameter larger than about one eighth of the column diameter and operated in gas and/or in supercritical chromatography [35–38]. The new Kinetex-C_{18} column represents a considerable (ca. 25%) improvement in column performance with a minimum reduced HETP around 1.1.

This is a remarkably low value, which redefines the limits of column packing technology. For the sake of comparison, a minimum value of about 0.5 was measured for a two dimensional array of porous silicon shell pillars that were perfectly organized, under similar experimental conditions, with a compound having a similar retention [39]. The thickness of the shell was 1.0 μm and the diameter of the pillars was 10 μm. The size distribution of the pillars was ideal, infinitely narrow ($d_{90/10} = 1$). The difference between this system and the bed of a Kinetex-C_{18} column is at least due to the disorder of a three-dimensional array being intrinsically higher than that of a two-dimensional array. Furthermore, the column bed is obtained by a slurry packing process instead of being etched as the pillar array. This analogy suggests, however, that the excep-
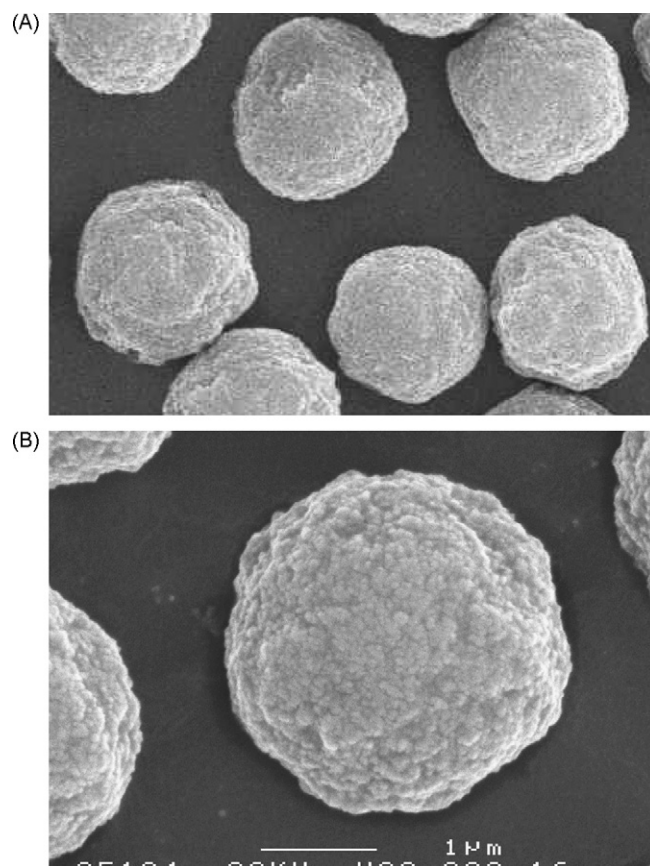
Fig. 4. Scanning electron microscopy (SEM) photographs of 2.7 μm Halo particles. (A) Collection of six particles. (B) Zoom in at the external surface of the particles. Note the irregular external surface area of these particles. Reproduced with permission of the manufacturer Advanced Material Technology.

tionally low eddy dispersion term of the Kinetex-C_{18} column like the low eddy dispersion term of the Halo-C_{18} column might be due to the unusually narrow particle size distribution of these shell particles. The manufacturers reported $d_{90/10}$ ratios of only 1.12 for the Kinetex-C_{18} particles and 1.14 for the Halo-C_{18} particles, while $d_{90/10}$ values are typically around 1.5–2.0 for totally porous particles. The performance of the Kinetex-C_{18} column may be better than that of the Halo-C_{18} columns, possibly due to the more closely spherical external shape of these particles as illustrated in Fig. 4A and B that show how the external surface of the 2.7 μm Halo-C_{18} particles is rough and irregular while Fig. 5A and B show that the external surface of the Kinetex-C_{18} particles is smooth at low scale. Magnified, however, the surface exhibits significant microscopic roughness, comparable to that of the Halo-C_{18} particle surface. From SEM photographs, it is impossible to derive even approximate estimates of the friction coefficient between particles and between particles and column wall. These frictions coefficients are critical in controlling the radial homogeneity of packed beds [40]. Fig. 5C shows that the porous shell thickness is uniform around the solid core. Its structure consists apparently in a series of 10 concentric layers of fine silica grains having an average size of about 25 nm. All these observations suggest that the short range eddies are probably smaller in the Kinetex-C_{18} than in the Halo column. This would be consistent with the HETP observations in Fig. 3A and B.

In Gidding's theory of eddy dispersion, the *A* term of packed beds is essentially accounted for by the flow heterogeneities between two adjacent particles (the so-called transchannel effect) that take place over a distance of one or two particle diameters (short-range interchannel effects) and across the column diameter (transcol-
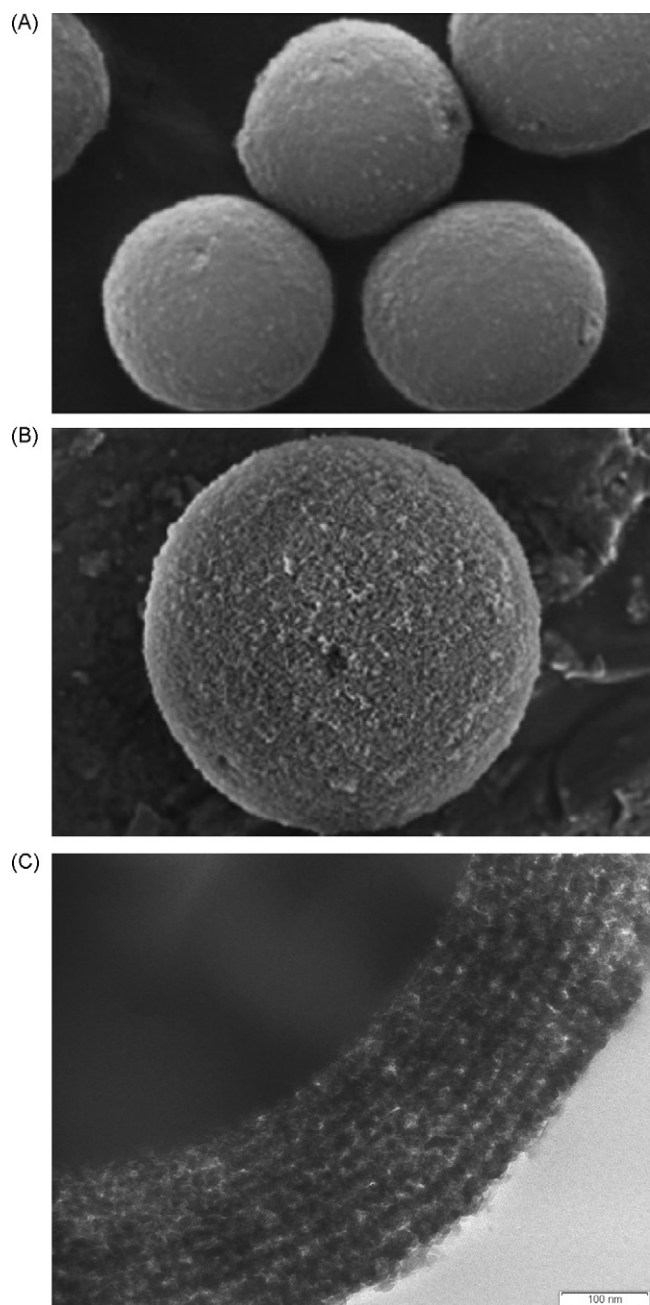
(A)

(B)

(C)

100 nm

Fig. 5. Same as in Fig. 4, except the particles are 2.6 μm (A and B) and 1.7 μm Kinetex particles (C). Note the apparent smoothness of the external surface area, the homogeneity of the thickness of the shell, and the structure (10–11 overlaid layers) within the porous shell. Reproduced with permission of Phenomenex, Torrance, CA.

umn effect). At high flow rates, the axial velocity along stream-path varies widely, which causes a strong axial dispersion of the bands, parts moving much faster than other parts that are close by. This causes important radial concentration gradients that are alleviated by both diffusion and eddy dispersion which consists in a flow exchange process of the sample molecules between these different streamlines of eluent with different axial velocities (the exchange diffusion process alone would be too slow). The sole contribution of the trans-channel effect was reproduced with a two-dimensional array of porous silicon shell pillars the center points of which were arranged on an equilateral triangular grid, with an interpillar porosity of 0.4 [39]. The reduced HETP of this array was 0.3 at infinite reduced linear velocity. According to Eq. (8), $\lambda_1 = 0.15$. The velocity difference between the center of the channels and the wall of

the particles was twice the average interstitial linear velocity $\bar{u}$, so $\omega_{\beta,1} = 1$ [21]. According to Eq. (9), the parameter $\omega_{\lambda,1} = 0.3$. The result of Malsche et al. means that the molecules of the sample are exchanged between the external surface area of the particles ($u = 0$) and the center of the interparticle channels ($u = 2\bar{u}$) over a distance of 0.3 particle diameter which is about the interparticle diameter, $0.3 \times d_p$. The short-range interchannel effect accounts for the local disorder of the packing at a scale of one particle diameter. So, the axial distance over which molecules are radially exchanged is between 1 and 2 particle diameters and $\omega_{\lambda,2} = 1.5$. Based on the narrow particle size distribution, the velocity difference, $\omega_{\beta,2}$, was estimated at 0.12 so $\lambda_2 = 0.01$.

Fig. 6A compares the theoretical (obtained as a combination of Eqs. (7), (8), (11), and (15)) and the experimental reduced HETPs of anthracene on the Kinetex and Halo columns. The Sherwood number Sh was estimated according to the Wilson and Geankoplis empirical correlation Eq. (14)[31]. The eddy dispersion parameters were $\lambda_1 = 0.1$ (see above), $\lambda_2 = 0.01$ (see above), and $\lambda_3 = 0$ (the long-range interchannel effect is neglected). The remaining parameters, Ω and $\omega_{\beta,c}$, were adjusted in order to match the experimental and the calculated h data by nonlinear multiple regression analysis. The results are listed in Table 2. We found $\Omega = 0.88$ and 0.59 on the Kinetex and the Halo columns, respectively. This is consistent with the fact that the porosity of the Halo-C_{18} shell ($\epsilon_p = 0.309$) is smaller than that of the Kinetex shell ($\epsilon_p = 0.444$). We found $\omega_{\beta,c,Kinetex} = 0.8\%$ and $\omega_{\beta,c,Halo} = 1.1\%$ (Table 2). Fig. 6B shows the same representation as in Fig. 6A, except that the sample is naphtho[2,3-a]pyrene, a more retained compound. For a given column, we observe in Table 2 an increase of the parameter Ω when the retention factor increases because surface diffusion increases as well [13]. Also, the impact of the transcolumn contribution ($\omega_{\beta,c}$ factor) decreases with increasing retention because there is more time for the sample to relax the radial concentration gradients across the column diameter, as demonstrated in [30].

In summary, the analysis of the reduced HETP of moderately retained, low molecular weight compounds in pure acetonitrile allows the derivation of estimates of the longitudinal diffusion term (B), the eddy dispersion term (A), and the C term of the new Kinetex-C_{18} column at high linear velocities (flow dispersion regime). The low value of $C = 0.04$ is essentially controlled by the external film mass transfer resistance (k_f), B is 1.46 (Eq. (7) with $\Omega = 0.90$, $k' = 0.5$), and $A = 0.6$. This contribution is most likely accounted for by the transchannel ($h_{Transchannel} = 0.3$) and the transcolumn velocity bias effects ($h_{Transcolumn} = 0.3$). Short-range interchannel effects are likely to be negligible due to the very narrow particle size distribution (PSD).

In the next section, we study the mass transfer kinetics of heavier and less diffusive compounds like peptides (bradykinin) and proteins (insulin and lyzozyme).

4.2.2. Peptide

The reduced HETP of bradykinin was first measured at ambient temperature, under slightly overloaded conditions. The pH of the eluent was set an acidic value by addition of 0.1% TFA to the mobile phase (acetonitrile and water, 23/77/0.1, v/v/v). Despite the small concentrations injected (0.2 g/L) and the wavelength used (205 nm), it was not possible to record strictly guassian peaks with a reasonable signal-to-noise ratio, i.e., a ratio above 10. Bradykinin has a positive charge (between +2 and +3, due to the presence of three proline and two terminal arginine amino acid residues). It strongly interacts with some specific adsorption sites, mostly unreacted silanol groups [41]. A significant degree of peak tailing was unavoidable and the thermodynamic contributions to band broadening bias the efficiency data. As a result, the h values reported in Fig. 3C, which are around 10, do not reflect accurately the actual efficiency of the two columns (see above). Nevertheless, it should
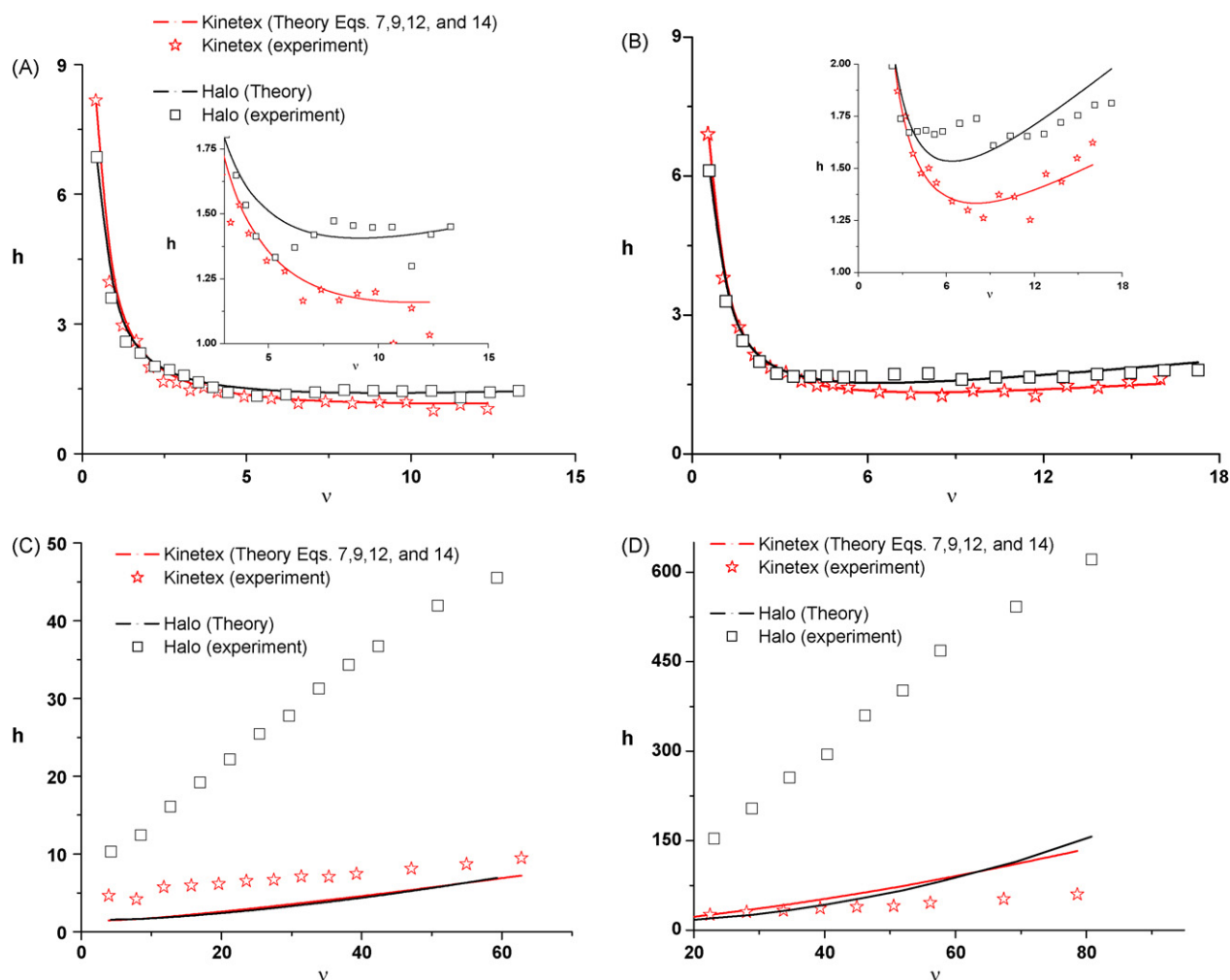
Fig. 6. Comparison between the experimental and the theoretical reduced HETPs of anthracene (A), naphtho[2,3-a]pyrene (B), insulin (C), and lyzozyme (D). The insert graph zooms in the high reduced linear velocity region in order to appreciate better the difference between the HETP data of each column. Note that all the experimental values of the C term measured with the Kinetex particles agree well with the calculated ones except in Fig. 4D where surface diffusion was neglected in the calculation (the parameter Ω is unknown for lyzozyme). The C terms of insulin and lyzozyme measured with the Halo particles are markedly larger than the theoretical one.

be emphasized that the C term remains negligible on the Kinetex column and that it is barely significant on the Halo column. This clearly demonstrates the ability of shell particles to provide extremely low solid-liquid mass transfer C terms with small peptides.

4.2.3. Proteins

Fig. 3D shows plots of the reduced HETP of insulin on Kinetex-C_{18} and Halo-C_{18}. Because the diffusion coefficient of insulin is about one order of magnitude smaller than that of small molecules, it is possible to perform measurements at much higher reduced velocities and to reach a range in which the C-terms of both columns can be estimated with a satisfactory precision. The high velocity branch of the Kinetex column ($C = 0.081$) is much flatter than that of the Halo column ($C = 0.666$). Yet, the average mesopore sizes of both brands of particles (90 and 96 Å) are similar, so the values of

the steric hindrance diffusion factor $F(\lambda)$ on both columns should be close. As previously measured on a similar porous medium and retentive conditions, the parameter Ω or ratio of the effective shell diffusivity to the bulk molecular coefficient should be close to 0.25 with $\epsilon_p = 0.43$ (Kinetex-C_{18}) [42]. One should expect a somewhat lower value of Ω, around 0.19 with shells having a smaller porosity $\epsilon_p = 0.31$ (Halo-C_{18}). The relative reduction of the C term compared to that of totally porous particles of the same size that we could expect is given by Eq. (15) and the values are 0.43 and 0.59 for the Kinetex ($\rho = 0.73$) and the Halo ($\rho = 0.63$) columns, respectively. Finally, the zone retention factor k_1 of insulin is about one and a half times larger on the Kinetex than on the Halo column. Overall, in theory (Eq. (15)), we should expect a ratio between the C terms of the Halo and the Kinetex columns close to 1.0 if the transparticle mass transfer resistance is the controlling kinetic event. The experimental ratio, however, is 8.3, a major deviation from this predicted value. The difference between the performance of the two columns must be found elsewhere. The manufacturer of Halo columns has consistently provided warnings regarding its application for large solutes. This poor behavior might result from a large external film mass transfer resistance between the interparticle moving eluent and the internal stagnant eluent with the Halo-C_{18} shell particles, from a strongly hindered intraparticle diffusion or from secondary interactions. Yet, no definitive answer has been brought to that question. The roughness of their external surface could possibly

Table 2
Best parameter Ω and ω_c obtained with anthracene and naphtha[2,3-a]pyrene.

	Anthracene		Naphtho[2,3-a]pyrene	
	Ω	ω_c (%)	Ω	ω_c (%)
Kinetex-C_{18}	0.90 ($k' = 0.4$)	0.8	1.16 ($k' = 1.4$)	0.4
Halo-C_{18}	0.61 ($k' = 0.5$)	1.1	0.91 ($k' = 2.8$)	0.5

be at the origin of this problem, large molecules such as proteins might have difficulties to find a direct pathway in and out of the particles, causing a large value of the external mass transfer coefficient. Further, detailed investigations which are necessary are in progress.

Fig. 6C compares the theoretical (Eqs. (7), (8), (11), and (15)) and the experimental reduced HETPs of insulin on the Halo and the Kinetex columns. The theoretical C term matches well the experimental C term of the Kinetex column. In contrast, the mass transfer kinetics between the mobile and the stationary phase on the Halo column is slow, which cannot be explained by theory on the basis of the classical transparticle and external film mass transfer resistances. Further detailed investigations are necessary to understand the unexpected, abnormal behavior of proteins on the Halo columns.

The same experiments were repeated but with a heavier, larger, and less diffusive protein, lysozyme. The results are shown in Fig. 3E. They confirm what has just been observed with insulin, e.g., a much smaller C term is measured on the Kinetex than on the Halo column. Again, the difference in the C term is of about one order of magnitude.

Fig. 6D compares the theoretical (Eqs. (7), (8), (11), and (15)) and experimental reduced HETPs of lysozyme on the Halo and the Kinetex columns. In the calculations, we estimated as follows the parameter Ω of lysozyme from [29], by omitting the contribution of surface diffusion:

$$\Omega = \frac{\epsilon_p^*}{\tau_p^{*2}} F(\lambda_m) \tag{19}$$

where ϵ_p^* and τ_p^* ($\simeq 1.3$ [43]) are the corrected porosity and tortuosity within the porous shell. Due to the relatively large ratio of the molecular diameter of lysozyme (42 Å) and the average pore size of the shells of Kinetex and Halo particles after C_{18} derivatization (77 and 72 Å, respectively), lysozyme is partially excluded from the mesopore network of these two particles. The parameter $F(\lambda_m)$ is the hindrance diffusion factor obtained from the Renkin correlation [44]:

$$F(\lambda_m) = (1 - \lambda_m)^2 (1 - 2.1044\lambda_m^2 + 2.089\lambda_m^3 - 0.948\lambda_m^5) \tag{20}$$

where λ_m is the ratio of the molecular size of the protein to the average mesopore size of the porous shell. Accordingly, $F(\lambda_m) = 0.14$ and 0.11 in the Kinetex-C_{18} and Halo-C_{18} particles, respectively. In combination with the ISEC data and the size of the polystyrene standards, lysozyme has then access to only 20% of the total porous volume of the shell [45].

We can now estimate the parameter Ω for lysozyme onto the Kinetex and Halo column. The retention factor, k', of lysozyme on Halo remains very small but varies between 0.02 and 0.40 (because retention factors of proteins depend strongly on the local pressure, a function of the flow rate), so the contribution of surface diffusion is likely small. According to Eq. (19), Ω is estimated at 0.20 (pore exclusion) $\times$ 0.309 (shell porosity) $\times$ 0.11 (hindrance diffusion factor) $\times$ (1/1.3^2) (channel's obstruction) = 0.0041. We found for the Kinetex column a value of 0.0072. However, we did not include the contribution of surface diffusion, which is unknown but may be significant because the retention factor of lysozyme on the Kinetex column varies between 0.5 and 1.6 [46].

Fig. 6C shows first that the calculated value of the C term matches well the best value derived from a fit to Eq. (6) of the experimental data of the Kinetex column for insulin. It is about three times larger with lysozyme because we did not account for the surface diffusion of this protein onto the Kinetex-C_{18} adsorbent in the expression of Ω. A perfect match would be obtained with $\Omega = 0.025$. Grossly, because surface diffusion accounts usually for at least 75% of the overall shell diffusivity for retained sample with $k' \simeq 1$ [42], one can reasonably estimate the parameter Ω as $4 \times 0.0072 = 0.0293$. This value would be consistent with the data measured with Kinetex.

Overall, the HETP data measured with the Kinetex column follow well the theoretical HETP presented in section 2.1. In contrast, the slow mass transfer kinetics between the mobile and the stationary phase observed on the Halo column cannot be explained by the theory on the basis of the classical transparticle and external film mass transfer resistances. The Wilson and Geankoplis correlation may not apply rigorously to the Halo column because the external surface of these particles is very rough and far from perfectly spherical. In contrast, the external surface area of the Kinetex poroshell particles shown by SEM photos is much smoother and well spherical. This could be a first interpretation. A second possible explanation for the excessively large reduced HETP of lyzozyme is based on the secondary interactions between the proteins insulin and lyzozyme with the Halo-C_{18} particles. Such interactions would be inexistent on Kinetex. Fig. 7A and B compare the peak shapes of insulin (flow rate of 1.2 mL/min) and lysozyme (flow rate of 0.9 mL/min), respectively, measured on the Kinetex and Halo columns. Regarding insulin, the Halo column provide better peak asymmetry at half their height around 1.3 *vs.* 1.5 for Kinetex. Hence, nor secondary interactions nor intraparticle diffusivity can explain the difference observed between Kinetex and Halo column with respect to the HETPs of insulin shown in Fig. 6C.
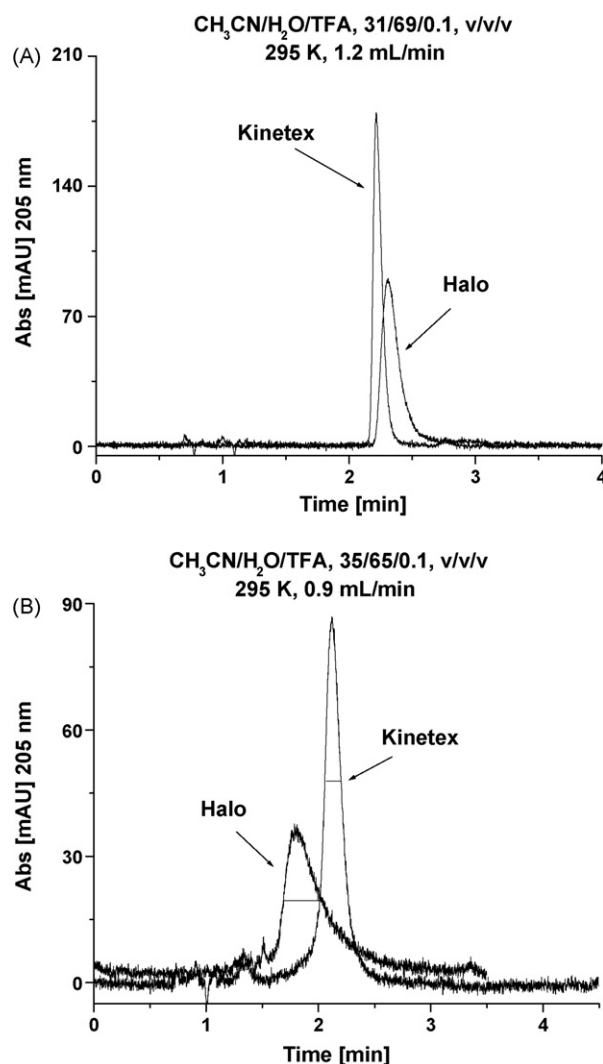

Fig. 7. Comparison between the peak shapes of insulin (A) and lysozyme (B) recorded on the Kinetex and Halo columns.
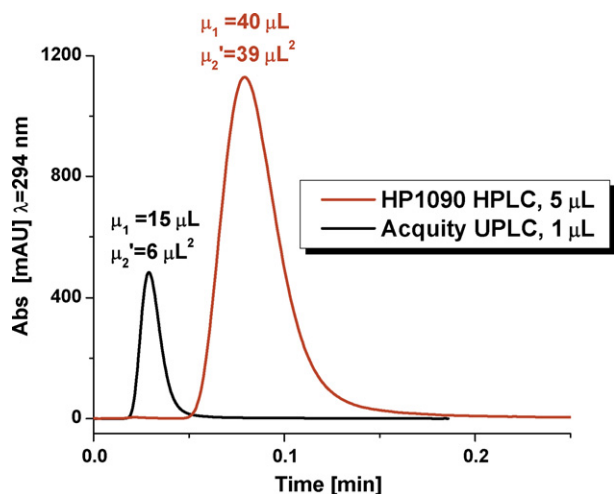
Fig. 8. Extra-column band profiles of naphtho[2,3-a]pyrene measured at a flow rate of 0.5 mL/min on the HP1090 (5 μL injection) and Acquity UPLC (1 μL injection) systems. Note the six times reduction of the second central moment when moving the column from the HP1090 to the Acquity UPLC after correction for the contribution of the volume injected to the second central moment (respectively 2.1 and 0.1 μL^2).

External film mass transfer is necessarily involved. In contrast, the half-height peak asymmetry of lyzozyme is significantly larger on the Halo (1.6) than on the Kinetex (1.2) columns. Secondary interactions clearly contribute to accentuate the HETP difference shown in Fig. 6D. At this point, one cannot comment more regarding the relatively poor C term measured on the Halo column with insulin and lysozyme.

4.3. Column performance and instrumentation

In the previous sections, we characterized the two columns studied by accurately measuring the amount of band broadening taking place in the column. The contributions of the extra-column volumes of the instrument used to the values of the first and second central moments of the recorded bands, that had been cautiously measured by replacing the column with a zero-volume connector. Then, these instrument moments were subtracted from the moments measured in the presence of the column.

The total first and second central moments measured for the sample band eluted through the column include the contributions of the injection volume, the sampling or injection device, the different connecting capillaries, the UV cell volume and the rate of signal-sampling applied. The corresponding characteristics of these contributions for the HP1090 and the Acquity UPLC liquid chromatographs are given in the experimental section. Fig. 8 illustrates the importance of these contributions and of the proper choice of the instrument on which to operate these new columns to benefit from their exceptional performance. This figure shows chromatograms of naphtho[2,3-a]pyrene recorded after percolating through the extra-column volume alone, at the same flow rate of 0.5 mL/min. This flow rate was chosen for the sake of achieving precise determinations. At the higher flow rate of 2 mL/min, the variance of the HP1090 instrument was 62 μL^2 while that of the Acquity remained unchanged at 6 μL^2. The first moment is proportional to the extra-column volume (40 μL *vs.* 15 μL for the HP1090 and the Acquity UPLC instruments, respectively, the extra-column variance contributions for naphtho[2,3-a]pyrene being 39 and 6 μL^2, respectively). The difference between the contributions of the two apparatus is significant. Should the total peak variances (including the extra-column and the column contributions) observed for a band be less than about five times the instrument contribution, the impact of the instrumentation on the overall col-

umn efficiency would be obvious [47]. It is difficult to achieve all the potential improvements in the resolution of difficult samples or in the speed of analysis that columns having exceptionally high levels of performance are used with instruments having significant extra column volumes. The chromatograph needs to be adapted to the level of efficiency of the columns used, otherwise the analyst will lose most of the possible gain in resolution power.

To illustrate this point, we need a compound the overall peak variance of which is of the order of 150 μL^2. For anthracene eluting from the 100 mm long Kinetex column on the Acquity UPLC and the HP1090 instruments at high flow rates (region where the C term is nearly negligible) these variances are 65 and 100 μL^2, respectively. For the 150 mm long Halo column, these variances are 125 and 170 μL^2, respectively. The larger peak variance of the Halo column is in part due to it being longer. Thus, the overall variances for a poorly retained compound ($k' \simeq 0.4$–0.5) are not much larger than the extra column contribution of the HP1090 system (39 μL^2). In contrast, they are slightly more than that 10 times that of the UPLC system (6 μL^2).

Fig. 9A shows the four HETP curves of anthracene measured with the Kinetex and the Halo columns on both instruments, before correction for the extra-column contributions (see Fig. 3A for the corrected data). It is interesting that, despite the Kinetex column having better intrinsic performance ($h_{min} = 1.1$) than the Halo col-
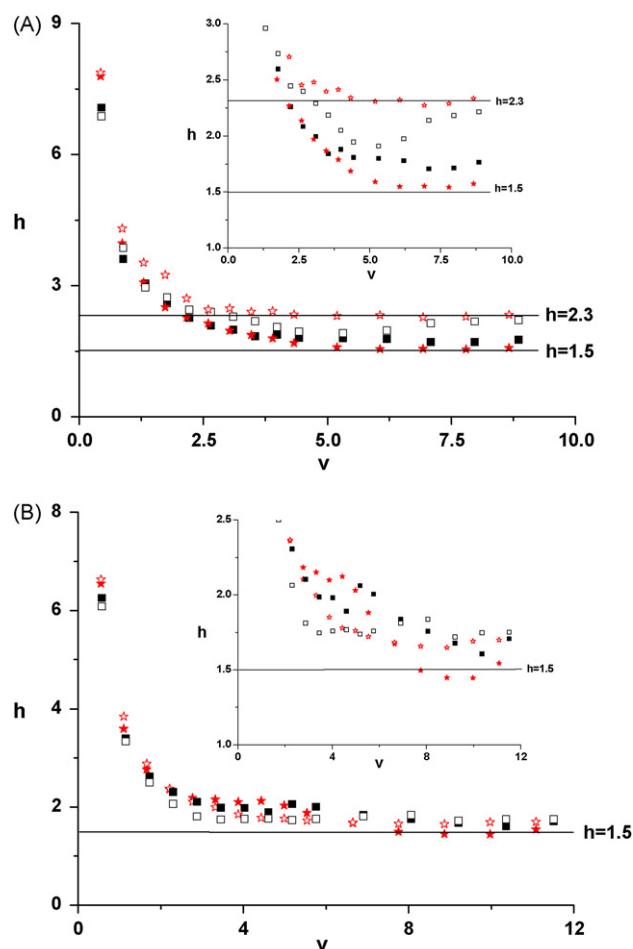

Fig. 9. Importance of the instrumentation used, HP1090 chromatograph (empty symbols) or Acquity chromatograph (full symbols), on the apparent efficiency of the Kinetex-C18 (stars) and the Halo-C18 (squares) columns before correction for the extra-column contributions. (A) Anthracene. (B) Naphtho[2,3-a]pyrene. The higher the retention of the sample, the smaller the impact of the extra-column volume contributions on the overall column efficiency.

umn ($h_{min} = 1.4$), the analyst could erroneously conclude that the two columns have similar reduced plate heights up to at least a reduced velocity of 10. This level of performance markedly exceeds that of totally porous particles operated with a HP1090 apparatus or any other of the same generations. The reduced HETPs measured at high flow rates for conventional packed RPLC columns are close to 2.2. The Halo column appears to perform better than the Kinetex column on the HP1090 because the actual peak variance measured with this instrument ($170\,\mu L^2$) is more than four times larger than the extra-column peak variance ($39\,\mu L^2$) while this ratio is only of 2.5 with the Kinetex column. In contrast, operating the Kinetex column with the Acquity UPLC instrument permits the analysts to benefit from the high performance of the Kinetex column because the extra-column contribution of this instrument is much smaller. An instrument with smaller extra column volumes would still improve further the practical usefulness of this column. The minimum reduced HETP values drop from 2.2 on the HP1090 apparatus to 1.5 and 1.8 on the Acquity for the Kinetex and the Halo columns, respectively. These values begin to approach those measured after correction from the extra-column contributions (1.1 and 1.4).

The situation is far more favorable for compounds having higher retention factors than anthracene, those that are of the order of those favored by analysts, between 2.5 and 5. One such compound is naphtho[2,3-a]pyrene ($k' \simeq 2$), which spends more time in the column and the peak of which has a larger variance at column outlet. The consequences of the extra-column contributions on the overall or apparent band broadening are markedly lower. The peak variances of naphtho[2,3-a]pyrene measured for the Kinetex column are 230 and $170\,\mu L^2$ on the HPLC and UPLC instruments, respectively. These values are 2.5 times larger than those for anthracene. They become 800 and $675\,\mu L^2$ for the Halo column. Fig. 9B shows plots similar to those in Fig. 9A, but for naphtho[2,3-a]pyrene. The difference between the uncorrected h values measured for Kinetex with the HP1090 ($h_{min} = 1.7$) and the UPLC Acquity ($h_{min} = 1.4$) instruments is markedly reduced. There is no longer any difference between the two sets of data for the Halo column ($h_{min} = 1.8$).

The performance of columns packed with modern, high efficiency shell particles has now become so high that it is limited by the characteristics of the instrument used to operate them. This limitation is particularly severe for poorly retained compounds, those that have the smallest variances, because the HETP of a column is proportional to its variance and variances are additive, The apparent efficiency of a peak that has a variance five times the variance contribution of the extra column volume is 20% less than the true column efficiency; if the peak variance is 10 times larger than the instrument contribution, the efficiency loss is still 10%, which seems to constitute an acceptable loss. In conclusion, the best instruments currently available are barely sufficient to use these columns and achieve the best performance that they potentially could make available. Current, conventional HPLC instruments are not designed to match the expected intrinsic resolution power of the best commercially available columns. The Kinetex column has dimensions ($4.6\,mm \times 100\,mm$) that allow its use on a HP1090 system but it eventually loses 50% ($h = 2.30$) of its maximum efficiency ($h_{min} = 1.15$) for weakly retained samples and still ca. 30% ($h = 1.70$) for moderately retained ones. In contrast, the efficiency losses are smaller on an Acquity UPLC system, 25% ($h = 1.55$) and 20% ($h = 1.45$), respectively.

4.4. Analytical applications

The separations of two moderately difficult samples, a mixture of oligostyrenes with 2–12 monomers and a polynuclear aromatic hydrocarbon mixture, were selected to illustrate the relative performance of the Kinetex-C_{18} column and that of the Luna C_{18} (HST) RPLC column.

4.4.1. Separation of oligostyrenes

The separation of oligostyrenes constitutes an excellent benchmark for HPLC because these samples have three different dimensions or attributes that are largely independent. These attributes can be used to investigate the separation power of chromatographic media or modes and of dimensionality. The first attribute, which is usually dominant, is the molecular weight (or degree of polymerization, n). The second sample attribute is the tacticity of each oligomeric fraction. The number of diastereomers in each such fraction increases as $2^{(n-2)}$. Thus, the tetramer has four diastereomers and the heptamer 32. The third attribute is chiral, each oligostyrene of given polymerization degree and tacticity has two enantiomers. The separation of the components of an oligostyrene sample depends on the selectivity of the system. For example, with methanol as the mobile phase, the separation is almost exclusively controlled by the molecular weight [48]. The retention of the oligomers increases according to the Martin rule [49]. In contrast, with acetonitrile, the diastereomer separations take place, albeit they are still largely controlled by the molecular weights [48]. Only when adsorption on a solid surface is used will the second attribute become independent of the molecular weight [48].

The separation of the oligostyrenes were used to compare the separation power of two $50\,mm \times 2\,mm$ columns, a Kinetex and a Luna C_{18}(HST) column. The characteristics of the Kinetex column were indicated earlier. The Luna column is packed with fully porous $2.5\,\mu m$ silica particles, with an average pore size of 10 nm and a surface area of $400\,m^2/g$ while that of Kinetex is only $100\,m^2/g$. The separations of the oligostyrene mixture were undertaken in three mobile phases, pure methanol under isocratic conditions, aqueous/methanol and aqueous/acetonitrile mobile phases, both under gradient conditions. The separation conditions were identical, with a flow rate of 0.2 mL/min under isocratic conditions and 0.4 mL/min under gradient conditions; in the case of the methanol system, a 12-min injection delay was included to limit the degree of migration in the isocratic region of operation. The injection volumes were 1 mL. The plot of $\log k'$ vs. n in Fig. 10 illustrates the linear relationship between the logarithm of the retention factor and the degree of polymerization for these oligostyrenes on both the Kinetex and the Luna columns. These plots were almost perfectly parallel, with
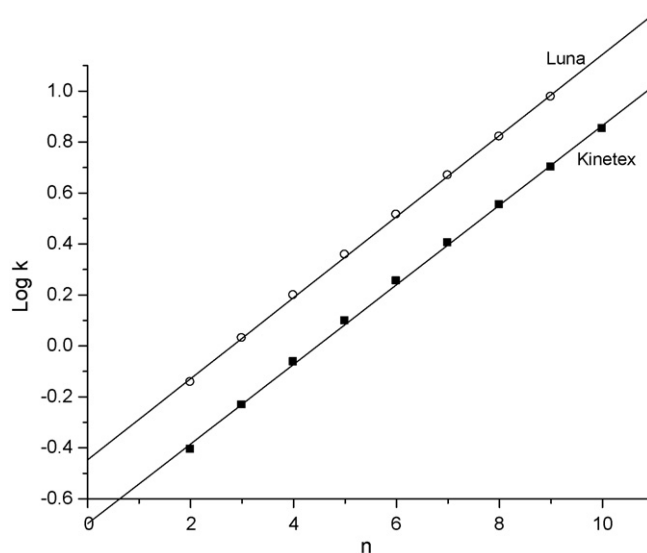

Fig. 10. Plot of $\log k'$ vs. n for the oligostyrenes eluting from the Kinetex column (■) and the Luna column (○). Mobile phases for both separations was 100% methanol, at 0.2 mL/min, injection volume μL, temperature 23 °C.
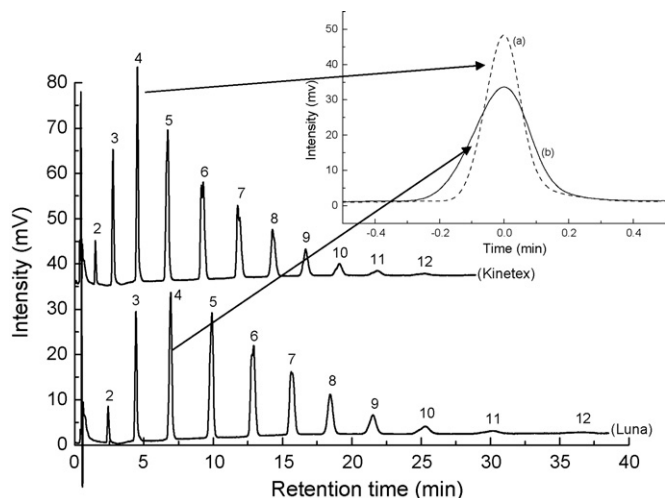
Fig. 11. Gradient elution separation of the oligostyrenes using an initial mobile phase of 10/90 water/methanol running to 100% methanol in 20 min at a flow rate of 0.4 mL/min. Injection delay, 12 min. Upper trace represents the separation on the Kinetex column, lower trace the Luna column. The inset illustrates the relative peak shape of the $n = 4$ oligomer on both columns. Data on the Kinetex column was offset 20 mV for visual clarity. Injection volume 1 μL, detection at 262 nm, temperature 23 °C.

slopes of 0.156 and 0.159 for the Kinetex and the Luna phases, respectively, thus indicating that both columns offer the same degree of peak discrimination, at least with respect to the identification of the peak retention time. They were, however, offset by an amount equivalent to almost two repeating units, with retention being greater on the Luna phase, consistent with the larger surface area. Effectively, the retention on the Luna phase was almost twice as long as that on the Kinetex column, for the same degree of peak to peak discrimination as that on the faster Kinetex column.

Operation of these columns under gradient conditions, with an initial mobile phase of 10/90 water/methanol running to 0/100 water/methanol in a 20-min period results in a very high resolution of the oligomeric separations on both columns, as shown in Fig. 10. Gradient conditions were employed in order to minimize the contributions to extra column band broadening since the void
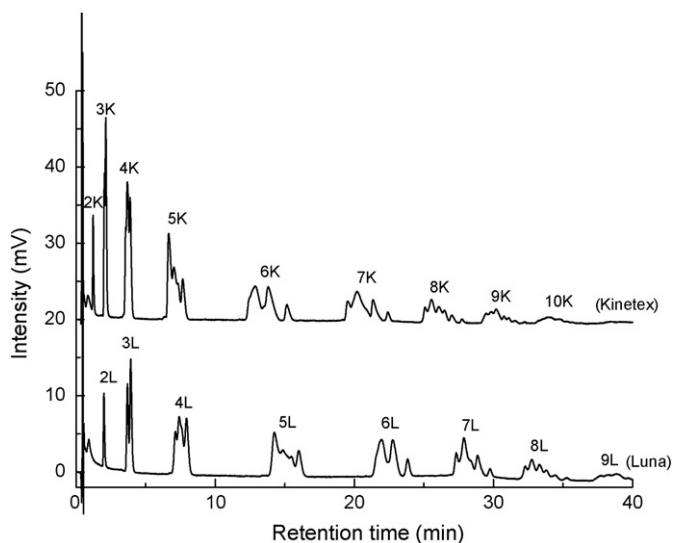

Fig. 12. Gradient elution separation of the oligostyrenes using an initial mobile phase of 10/90 water/acetonitrile running to 100% acetonitrile in 20 min at a flow rate of 0.4 mL/min. Upper trace represents the separation on the Kinetex column, lower trace the Luna column. Data on the Kinetex column was offset 20 mV for visual clarity. Injection volume 1 μL, detection at 262 nm, temperature 23 °C.
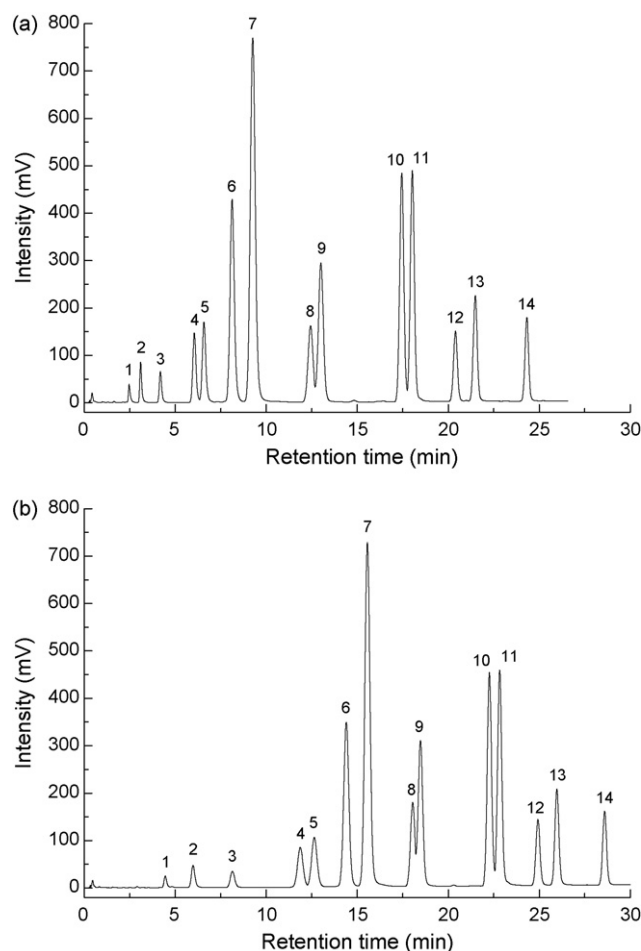

Fig. 13. Separation of a mixture of PAHs on the RPLC C_{18}-bonded packed columns (A) Kinetex and (B) Luna, using gradient elution: mobile phase A = 60/40 water/acetonitrile running to 100% acetonitrile at 1%/min. Flow rates, 1.0 mL/min. Detection at 254 nm. Injection volumes 5 μL. Peaks are assigned in the following order: (1) 2,2-binaphthyl, (2) naphthalene, (3) acenaphthylene, (4) acenaphthene, (5) fluorene, (6) phenanthrene, (7) anthracene, (8) fluoranthene, (9) pyrene, (10) chrysene, (11) 1,2-benzanthracene, (12) benzo[e]pyrene, (13) benzo[a]pyrene, (14) benzo[g,h,i]perylene.

volume of the instrument is large relative to the small volume of these short, narrow bore columns. An injection delay was employed to limit any isocratic elution behavior. Some diastereomer separations were apparent for several of the oligomer fractions, mostly for $N = 5$. Qualitative assessment of these chromatograms shows a markedly increased sensitivity of the Kinetex column at the same gradient rate, consistent with a narrow elution band on the Kinetex column. It should be noted that the retention of the oligomers is substantially less on the Kinetex than on the Luna column. The $n = 4$ oligomer for example eluted almost 35 specific surface areas of the two phases. However, this decrease in retention does not reflect a decrease in the separation performance of the Kinetex column, which is actually superior to that of the Luna column (see inset in Fig. 11 of the $n = 4$ oligomer fraction, which shows increased peak height and deceased band broadening on the Kinetex column), as apparent also in the separation of the polyaromatic nuclear hydrocarbons detailed in the following section.

The separations obtained using acetonitrile mobile phases (gradient elution from 10/90 water/acetonitrile to 0/100 water/acetonitrile in 20 min) (Fig. 12) shows very similar separation power for both columns, but with a reduction in separation time of 23 Kinetex column.

4.4.2. Separation of a typical mixture of polynuclear aromatic hydrocarbons

The separation of mixtures of polynuclear aromatic hydrocarbons (PAH) provides an important challenge in environmental analyses. To test the separation power of the Kinetex column and compare its analytical performance to those of more conventional packed RPLC columns, we chose a relatively simple sample containing only 14 components, but a challenging one that contains three pairs of structurally similar compounds (fluoranthene/pyrene with length to breadth ratios of approximately 1.34 and 1.43, chrysene/1,2-benzanthracene with length to breadth ratios of approximately 1.71 and 1.75, and acenaphthene/fluorene). We analyzed this mixture on two 50 mm × 2.1 mm columns, the Kinetex-C_{18} and the Luna C_{18} HST, supplied by Phenomenex.

The chromatograms in Fig. 13 illustrate the separations that were achieved on each of the two columns. An extensive optimization process was not undertaken. Instead, the experimental conditions were chosen in order to achieve the separation of all 14 components in the shortest possible time on at least one of the columns, with $R > 1$. Then, the separation was repeated on the other column using these same conditions, so the same conditions were used on both columns. These conditions used an initial mobile phase of 60/40 water/acetonitrile and a gradient to 100% acetonitrile at 1.5%/min, at a flow rate of 0.4 mL/min. We did not optimize the superficial fluid velocity. All 14 PNAs were baseline resolved on the Kinetex column, in less than 25 min. The peak capacity of this separation defined as the ratio of the duration of the analysis to the average baseline width of the eluted peaks was 88.

Under the same conditions the Luna C_{18} column resolved 14 components but with a resolution of peaks 8 and 9 less than 1 and a total analysis time of 29.5 min. The peak capacity of this separation was 58, due to the increased band width of the eluted peaks. The Kinetex column was therefore 8% faster at the same pressure) and yielded a greater resolving power. In fact, the separation speed of the Kinetex column, up to the elution of the limiting peak pair (8 and 9) was 28.

5. Conclusion

Our results demonstrate the excellent performances of a new brand of columns packed with shell particles (Kinetex-C_{18}) under isocratic conditions. These particles consist of a 1.9 μm diameter solid core covered by a regular 0.35 μm porous shell. A 4.6 mm × 100 mm I.D. column packed with this material showed experimental minimum HETPs as low as 1.1 with small molecules, using pure acetonitrile as the eluent. In comparison, the minimum HETP of the commercially available 4.6 mm × 150 mm Halo column, also packed with shell particles, is 1.4 under the same experimental conditions. Never had such a low reduced HETP value been achieved in column manufacturing technology. SEM photographs of Kinetex-C_{18} particles would suggest that this high performance results from a significant improvement in the characteristics of the shell particles. The Kinetex-C_{18} particles seem to have a very narrow size distribution ($d_{90/10} = 1.12$), they are nearly spherical, with a smooth external surface and a uniform shell thickness around the solid core. In contrast, the Halo-C_{18} particles do not have a smooth spherical shape and their external surface is rough and irregular.

Compared with classical fully porous silica particles, the exceptional performance of the Kinetex column is due a significant reduction in the eddy dispersion or A term and to a lower term of mass transfer resistance between the mobile and the stationary phase. Due to the narrow particle size distribution of the Kinetex-C_{18} particles, the short-range interchannel velocity biases are reduced. The transchannel ($h = 0.2$) and transcolumn ($h = 0.4$) velocity biases remain the responsible for the velocity biases in Kinetex columns. For reasons not yet understood, the C term of the Kinetex column

is much smaller than that of the Halo column for proteins and it is in excellent agreement with theoretical predictions of the value of this term when it is accounted for by the transparticle and the external film mass transfer resistances for spherical shell particles. However, one can definitely not assess the intrinsic performance of a column when the extra-column variance contribution of the instrument is significant compared to the variance measured with the column and when the retention factor is small.

This new type of shell particles is a new landmark in the preparation of better particles for HPLC. It does looks extremely promising. However, further work remains necessary better to characterize the chromatographic behavior of the Kinetex columns, to investigate the origin of the peculiar properties, like the low values of the A and C terms, to evaluate the peak capacity in gradient elution and its dependence on the gradient time. Further work is in progress in these areas.

Nomenclature

Roman letters

A	eddy diffusion term in the reduced van Deemter Eq. (5)
B	longitudinal diffusion coefficient in the reduced van Deemter Eq. (5)
C	liquid–solid mass transfer coefficient in the reduced van Deemter Eq. (5)
d_p	average particle size (m)
D_m	bulk molecular diffusion coefficient (m^2/s)
D_{Shell}	effective molecular diffusion coefficient in the porous shell (m^2/s)
$F(\lambda_m)$	pore steric hindrance parameter
F_v	inlet flow rate (m^3/s)
H	total column HETP (m)
h	total reduced column HETP
$h_{Long.}$	contribution of longitudinal diffusion to the total reduced HETP
h_{Eddy}	contribution of eddy diffusion to the total reduced HETP
h_{Film}	contribution of the external film mass transfer resistance to the total reduced HETP
$h_{Particle}$	contribution of the transparticle mass transfer resistance to the total reduced HETP
K_a	Henry's constant
K_c	Kozeny–Carman constant
k'	retention factor
k_f	external film mass transfer coefficient (m/s)
k_1	particle retention factor in a core-shell particle
L	column length (m)
M	molecular weight of the analyte (g/mol)
M_S	molecular weight of the eluent (g/mol)
ΔP	column pressure drop (Pa)
R_i	radius of the solid silica core (m)
R_e	particle radius (m)
R_c	column inner radius (m)
Sh	Sherwood number
T	temperature (K)
$t^f_{1/2}$	elution time measured at the front half-height of the peak in presence of the column (s)
$t^r_{1/2}$	elution time measured at the rear half-height of the peak in presence of the column (s)
$t^f_{1/2,e}$	elution time measured at the front half-height of the peak in absence of the column (s)
$t^r_{1/2,e}$	elution time measured at the rear half-height of the peak in absence of the column (s)
t_R	elution time of the apex of the peak in presence of column (s)

t_e	elution time of the apex of the peak in absence of column (s)
u	interstitial linear velocity (m/s)
u_S	superficial linear velocity (m/s)
V_A	molar volume of the solute at its boiling point ($m^3.mol^{-1}$)

Greek letters

η	eluent's viscosity (Pa s)
ϵ_e	external column porosity
ϵ_p	porosity of the porous shell
ϵ_p^*	porosity of the shell for partially excluded proteins
ϵ_t	total column porosity
γ_e	external obstruction factor
λ_m	ratio of the hydrodynamic radius of the analyte to the mesopore radius
λ_i	eddy dispersion coefficient related to a flow exchange mechanism for a velocity bias of type i
$\mu'_{2,ex}$	second central moment of the extra-column band profiles (s^2)
ν	reduced interstitial linear velocity of the eluent to the particle diameter d_p and bulk molecular diffusion coefficient D_m
ω_i	eddy dispersion coefficient related to a diffusion exchange mechanism for a velocity bias of type i
$\omega_{\beta,c}$	relative velocity difference between the center and the wall of the column tube
$\omega_{\beta,i}$	relative velocity inequality for a velocity bias of type i
$\omega_{\lambda,i}$	reduced axial flow length for a velocity bias of type i reported to the particle diameter d_p
Ω	ratio of the intraparticle diffusivity of the sample through the porous shell to the bulk diffusion coefficient
Ψ	association factor of the eluent
ρ	ratio of the diameter of the solid core to that of the particle in a core-shell particle
τ_p^*	tortuosity factor of the porous shell for partially excluded protein

Acknowledgements

References

[1] 32nd International Symposium on High Performance Liquid Phase Separations and Related Techniques, Baltimore, MD, May 10–16, 2008.
[2] F. Gritti, G. Guiochon, J. Chromatogr. A 1216 (2009) 1353.
[3] Pittcon Conference & Expo 2009, Chicago, IL, March 8–13, 2009.
[4] J. Kirkland, Anal. Chem. 41 (1969) 218.
[5] J. Kirkland, Anal. Chem. 64 (1992) 1239.
[6] J. Kirkland, F. Truszkowski, C. Dilks, G. Engel Jr., J. Chromatogr. A 890 (2000) 3.
[7] J. Knox, J. Vasvari, J. Chromatogr. 83 (1973) 181.
[8] X. Wang, W. Barber, P. Carr, J. Chromatogr. A 1107 (2006) 139.
[9] F. Gritti, G. Guiochon, J. Chromatogr. A 1157 (2007) 289.
[10] K. Kaczmarski, G. Guiochon, Anal. Chem. 79 (2007) 4648.
[11] A. Cavazzini, F. Gritti, K. Kaczmarski, G. Guiochon, Anal. Chem. 79 (2007) 5972.
[12] J. Abia, K. Mriziq, G. Guiochon, J. Chromatogr. A 1216 (2009) 3185.
[13] F. Gritti, G. Guiochon, AIChE J., AICHE-09-11844, in press.
[14] F. Gritti, G. Guiochon, J. Chromatogr. A 1216 (2009) 4752.
[15] C. Wilke, P. Chang, AIChE J. 1 (1955) 264.
[16] B. Poling, J. Prausnitz, J. O'Connel, The Properties of Gases and Liquids, 5th ed., McGraw-Hill, New York, NY, 2001.
[17] M. Young, P. Carroad, R. Bell, Biotechnol. Bioeng. 22 (1980) 947.
[18] W. Bocian, J. Sitkowski, E. Bednarek, A. Tarnowska, R. Kawecki, L. Kozerski, J. Biomol. NMR 40 (2008) 55.
[19] I. Nesmelovai, V. Fedotov, Biochim. Biophys. Acta 1383 (1998) 311.
[20] J. van Deemter, F. Zuiderweg, A. Klinkenberg, Chem. Eng. Sci. 5 (1956) 271.
[21] J. Giddings, Dynamics of Chromatography, Marcel Dekker, New York, NY, 1965.
[22] C. Horvath, H.-J. Lin, J. Chromatogr. 126 (1976) 401.
[23] C. Horvath, H.-J. Lin, J. Chromatogr. 149 (1978) 43.
[24] G. Guiochon, A. Felinger, A. Katti, D. Shirazi, Fundamentals of Preparative and Nonlinear Chromatography, 2nd ed., Academic Press, Boston, MA, 2006.
[25] D. Ruthven, Principles of Adsorption and Adsorption Processes, Wiley, New York, NY, 1984.
[26] M. Suzuki, Adsorption Engineering, Elsevier, Amsterdam, The netherlands, 1990.
[27] K. Miyabe, G. Guiochon, J. Sep. Sci. 26 (2003) 155.
[28] J. Knox, L. McLaren, Anal. Chem. 36 (1964) 1477.
[29] F. Gritti, G. Guiochon, Anal. Chem. 78 (2006) 5329.
[30] F. Gritti, G. Guiochon, AIChE J., AICHE-09-11893, in press.
[31] E. Wilson, C. Geankoplis, J. Ind. Eng. Chem. (Fundam.) 5 (1966) 9.
[32] F. Gritti, G. Guiochon, J. Chromatogr. A 1166 (2007) 30.
[33] D. McCalley, J. Chromatogr. A 1193 (2008) 85.
[34] J. Knox, J.F. Parcher, Anal. Chem. 41 (1969) 1599.
[35] R.T. Kennedy, J.W. Jorgenson, Anal. Chem. 61 (1989) 1128.
[36] L.J. Cole, N.M. Schultz, R.T.J. Kennedy, J. Microcolumn. Sep. 5 (1993) 433.
[37] Y. Shen, M.L. Lee, Anal. Chem. 69 (1997) 2541.
[38] Y. Shen, M.L. Lee, Anal. Chem. 70 (1998) 737.
[39] W. de Malsche, H. Gardeniers, G. Desmet, Anal. Chem. 80 (2008) 5391.
[40] G. Bee, J. Ureta, R. Shalliker, E. Drumm, G. Guiochon, AIChE J. 49 (2003) 642.
[41] F. Gritti, G. Guiochon, Anal. Chem. 81 (2009) 9871.
[42] F. Gritti, G. Guiochon, Anal. Chem. 81 (2009) 2723.
[43] F. Gritti, G. Guiochon, Chem. Eng. Sci. 61 (2006) 7636.
[44] E. Renkin, J. Gen. Physiol. 38 (1954) 225.
[45] F. Gritti, G. Guiochon, J. Chromatogr. A 1176 (2007) 107.
[46] K. Miyabe, G. Guiochon, J. Phys. Chem. B 108 (2004) 2987.
[47] F. Gritti, A. Felinger, G. Guiochon, J. Chromatogr. A 1136 (2006) 57.
[48] M. Gray, A.P. Sweeney, G.R. Dennis, P. Wormell, R.A. Shalliker, J. Liq. Chromatogr. Relat. Technol. 27 (2004) 2905.
[49] A.J.P. Martin, Biochem. Soc. Symp. 3 (1949) 4.
[50] T. Farkas, M.J. Sepaniak, G. Guiochon, AIChE J. 43 (1997) 1964.